OSIRIS observations of a tongue of NO_x in the lower stratosphere at the Antarctic vortex edge: comparison with a high-resolution simulation from the Global Environmental Multiscale (GEM) model[1]

C.E. Sioris, S. Chabrillat, C.A. McLinden, C.S. Haley, Y.J. Rochon, R. Ménard, M. Charron, and C.T. McElroy

Abstract: Selected NO_x profiles of the Antarctic lower stratosphere inferred from OSIRIS NO_2 observations are presented from the austral spring of 2003. These observations show a tongue of NO_x at 100 hPa, with a concentration typical of the middle stratosphere. Simulations with the Global Environmental Multiscale model show that this small-scale tongue of NO_x-rich air descended into the lower stratosphere. The tongue was formed as a result of a Rossby wave breaking days earlier, transporting NO_x from the pole, where larger concentrations had recently appeared, to the edge of the vortex. The three-dimensional structure of the breaking wave is illustrated in detail.

PACS Nos.: 92.60.hf, 92.60.Xg, 93.30.Ca

Résumé : Nous présentons des profils choisis de NO_x dans la basse stratosphère de l'Antartique obtenus des observations de NO_2 d'OSIRIS pendant le printemps austral de 2003. Ces observations montrent une bande de NO_x à 100 hPa, avec une concentration typique de la stratosphère moyenne. Des simulations avec le modèle Global Environmental Multiscale montrent que cette petite bande d'air riche en NO_x est descendue dans la basse stratosphère. La bande s'est formée quelques jours auparavant, résultant d'un bris d'onde de Rossby, transportant le NO_x en provenance du pôle où de grandes concentrations sont apparues récemment, jusqu'au bord du vortex. Nous illustrons en détail la structure 3-D du bris d'onde.

[Traduit par la Rédaction]

Received 3 April 2007. Accepted 23 July 2007. Published on the NRC Research Press Web site at http://cjp.nrc.ca/ on 17 October 2007.

C.E. Sioris,[2] C.A. McLinden, Y.J. Rochon, and C.T. McElroy. Atmospheric Science and Technology Directorate, Environment Canada, 4905 Dufferin St., Toronto, ON M3H 5T4, Canada.
S. Chabrillat. Belgian Institute for Space Aeronomy, 3 avenue Circulaire, 1180 Brussels, Belgium.
C.S. Haley. York University, 4700 Keele St., Toronto, ON M3J 1P3, Canada.
R. Ménard and M. Charron. Atmospheric Science and Technology Directorate, Environment Canada, 2121 Trans-Canada Highway, Dorval, QC H9P 1J3, Canada.

[1]This original article is from work that highlights some of the science that has been produced in the last couple of years using the Odin satellite.

[2]Corresponding author (e-mail: Christopher.Sioris@ec.gc.ca).

 doi: 10.1139/P07-123

Introduction

NO_2 profile observations in the polar lower stratosphere are very difficult to interpret because they are influenced by dynamics, heterogeneous and gas-phase photochemistry, cloud sedimentation, and even sometimes mesospheric processes related to solar activity. Interpretation of these observations is made easier by first converting the measurements to NO_x ($NO + NO_2$) using a photochemical model (see, for example, ref. 1). Then, the NO_x derived from the observations can be compared directly with simulated NO_x from a three-dimensional chemical transport model such as the Global Enviromental Multiscale (GEM) model.

In this paper, we use GEM simulations to study, in detail, a tongue of NO_x observed by OSIRIS (Optical Spectrograph and Infrared Imager System) [2] as it circulates just inside the Antarctic vortex edge. The motivation for this study was to explain one of several OSIRIS observations of enhanced lower stratospheric NO_2 in this region in early austral spring. A second motivation is to simply show the variability in lower stratospheric NO_x at polar latitudes due to dynamical processes. This can be important for remote sensing methods that assume zonal gradients in stratospheric NO_2 are relatively weak (see, for example, ref. 3) in attempting to measure the tropospheric column abundance. An example of a similar study of the signatures of planetary wave breaking in satellite-based limb measurements of stratospheric chemical composition was conducted by Leovy et al. [4], who used O_3 profile data from the Limb Infrared Monitor of the Stratosphere (LIMS) and focused on the middle stratosphere ($\leq$30 hPa).

Method

OSIRIS (onboard the Odin satellite) measures limb-scattered sunlight in the 280–810 nm range. The 435–450 nm interval is used to retrieve vertical profiles of NO_2 down to $\sim$10 km with 2 km vertical resolution. Measurements of approximately the same volume of air occur every 12 h (at $\sim$6 a.m. and p.m. local time) if sunlight is present. The vertical sampling, provided by the nodding satellite, is 2 km and covers a nominal tangent height range of 7–70 km. The latitudinal and longitudinal sampling of OSIRIS are typically 5° and 25°, respectively. The fine latitudinal sampling provides a cross-sectional view of a chemical field (i.e., altitude versus latitude at near constant longitude) with sufficient resolution to see small-scale ($\sim$1000 km) wave structures along this plane. Odin's orbital period is 96 min [5], so multiple views of atmospheric phenomena stretching over 25° of longitude are possible in quick succession. OSIRIS NO_2 has been validated to 20% [6].

We have searched through 2 years (May 2003 – May 2005) of OSIRIS version 2.4 NO_2 profiles [7] for local maxima (enhancements) in the 10–46 km range. An enhancement is deemed present if the observed NO_2 volume mixing ratio (VMR) at a given altitude minus its 1σ uncertainty is greater than the VMR plus the 1σ uncertainty for the immediately overlying layer, or if there is an order-of magnitude enhancement relative to photochemical model [1] simulations for the same local time, latitude, month, and altitude. In addition, the profile must show a minimum NO_2 number density of $<10^9$ molecules/cm^3 below 20 km. The latter criterion was included as a simple means of ensuring that the profile had concentrations in the lowermost polar stratosphere that are representative of wintertime conditions. Without this criterion, many cases of poleward transport of NO_2 from midlatitudes would be included from the vortex breakup period in midspring. We have also removed cases from high latitudes ($|\text{lat}| > 60°$) since they may be primarily caused by renitrification from the vaporization of particles containing odd nitrogen (for example, nitrates). The preceding criteria effectively bring the focus of the search on the vortex edge region in polar winter and spring, without imposing time period constraints.

The OSIRIS radiance (Level 1) data are reanalyzed using the retrieval method of Sioris et al. [8, 9] because the Level 1 version used to retrieve the version 2.4 NO_2 had pointing information biased by $\sim$1 km [6]. The Level 1 data have since been corrected and version 3.0 NO_2 has been retrieved for the entire mission [10]. However, version 3.0 often lacks data at the lowest retrieval altitudes due to

Table 1. OSIRIS observations of large enhancements in the lowermost stratospheric vortex edge region. The difference in NO_2 VMR between the local maximum and the nearest overlying local minimum is 'dVMR'. Longitude is abbreviated as "long.".

Year	Month	Day	UTC (hh:mm)	z (km)	p (hPa)	lat. (°)	long. (°)	VMR (pptv)	dVMR (pptv)
2003	9	19	15:15	14	140	−48	36	331	5
2003	9	26	09:39	13	151	−58	124	288	63
2003	10	13	16:23	15	119	−60	−163	485	365
2003	10	13	22:51	17	75	−58	101	501	229
2003	10	14	05:15	13	144	−59	4	213	71
2003	11	16	04:33	15	112	−56	13	186	62
2004	11	15	23:55	15	114	−51	88	220	20
2005	3	14	16:25	16	91	55	19	359	8

oversensitive cloud identification and overly stringent data filtering [10].

The conversion from NO_2 to NO_x is achieved with photochemical box model [1] simulations, constrained by profiles of the European Centre for Medium-Range Weather Forecasts (ECMWF) [11] temperature (temperature profiles are from ECMWF) and ozone profiles measured by OSIRIS [12]. The NO_x/NO_2 ratio from the model simulations is used to scale OSIRIS NO_2 to NO_x. The ratio is appropriate for the altitude, time of day, year, and latitude of the OSIRIS measurements (see also ref. 13).

The GEM model is used to interpret the OSIRIS observations. GEM is a forecasting model developed at the Meteorological Service of Canada and integrated into a 4D-var assimilation system to deliver weather forecasts operationally. Here, we use a research version, named GEM-BACH, which runs on a global uniform grid with 1.5° × 1.5° horizontal resolution, 80 levels extending from the surface up to 0.1 hPa with a vertical resolution of 5 hPa in the lower stratosphere. Among many changes since the model description [14], this version includes many updates and improvements of the physical parameterizations to allow adequate modelling of stratospheric dynamics and a new module (BACH, Belgian Atmospheric CHemistry) to integrate online the chemical composition of the stratosphere. This stratospheric chemistry module was developed originally for BASCOE, a stratospheric chemistry-transport model [15] and assimilation system [16]. The time step of the module is 45 min.

In this study, the assimilation system processes, in 6 h time windows, the usual set of meteorological observations. No assimilation of chemical observations was performed for the present study. Hence, the chemical output is very similar to the result of a Chemistry-Transport Model (CTM) driven offline by meteorological analyses, with the model state saved in 6 h increments.

Observations and simulations

We find several cases where a dynamical disturbance has clearly led to enhancements of NO_2 in the lower stratosphere in the polar spring (see Table 1). It is clear that many other such cases exist in the OSIRIS data record, but they have been filtered out by the aforementioned criteria of the simple automated search. Pressure (p) data in Table 1 are from ECMWF [11]. We focus hereafter on the third case listed in Table 1, which provided the largest VMR enhancement.

A breaking Rossby wave caused an intrusion or tongue of high NO_x concentrations that stretched into the vortex edge region of the lower stratosphere at a pressure of ∼85 hPa (Fig. 1*a*). The tongue shows its first sign of intensity in GEM-simulated NO_x fields at 18:00 UTC on 8 October 2003 (not shown) as it extends from the South Pole toward the vortex edge. The intensity of this dynamical event steadily increases during 9 October. The tongue is clearly present at 00:00 UTC on 9 October 2003 (Fig. 1*a*) and is advected eastward in the large-scale flow by 12:00 UTC (not shown). By 00:00 UTC on 10 October, the wave breaking event has passed (not shown), but NO_x continues to be advected eastward

Fig. 1. (*a*) (Top left) Map of NO_x VMR (pptv) in the southern hemisphere collar and polar regions at 85 hPa on 9 October 2003 at 00:00 UTC. (*b*) (Top right) same as (*a*), except for 12:00 UTC on 10 October, and $p = 90$ hPa. (*c*) (Middle left) same as (*a*), except for 00:00 UTC on 12 October, and $p = 100$ hPa. (*d*) (Middle right) same as (*a*), but for 12:00 UTC on 12 October and $p = 120$ hPa. (*e*) (Bottom left) same as (*a*), but for 12:00 UTC on 13 October, and $p = 150$ hPa. The pressure in this sequence of GEM snapshots is varied to match the central pressure of the NO_x enhancement (at 65°S). White arrows and rings are used to draw the reader's attention to the feature of interest.

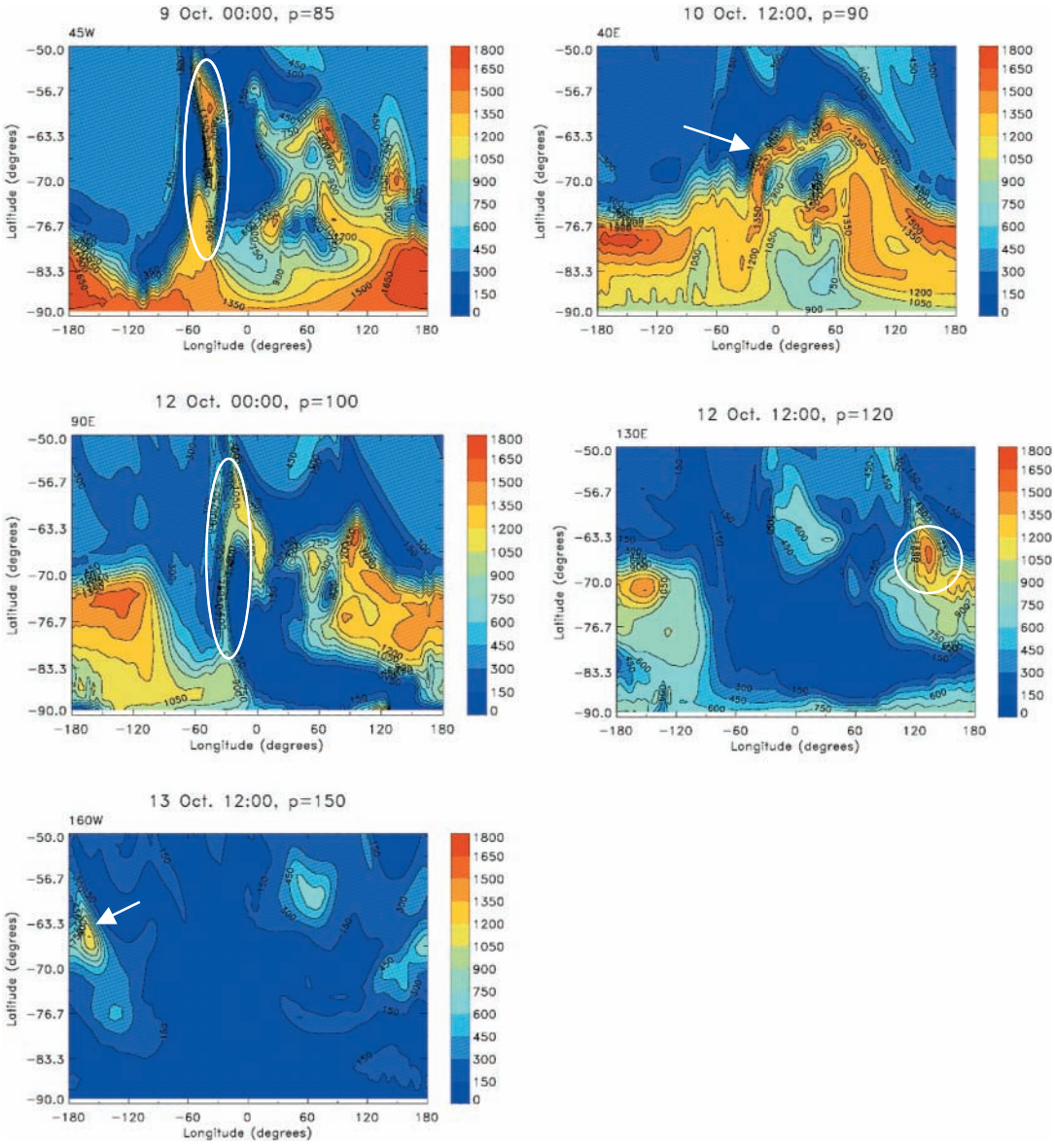

(Fig. 1*b*) on this day. By 00:00 UTC on 12 October, a second breaking wave can be seen (Fig. 1*c*) at a similar longitude (30°W) as the first. At this longitude, the wind direction has a strong equatorward component between 75 and 65°S (see example below), which lasts for many days, whereas at all other

Fig. 2. "Snapshot meridional" cross section of NO_x VMR (pptv) obtained from an orbit of OSIRIS on 13 October 2003 between 15:39 and 16:41 UTC. The enhancement observed during the scan at 60°S was at 163°W at 16:23 UTC. Areas in black could not be retrieved due to cloud interference. For areas in white, $[NO_x] > 1.5$ ppbv.

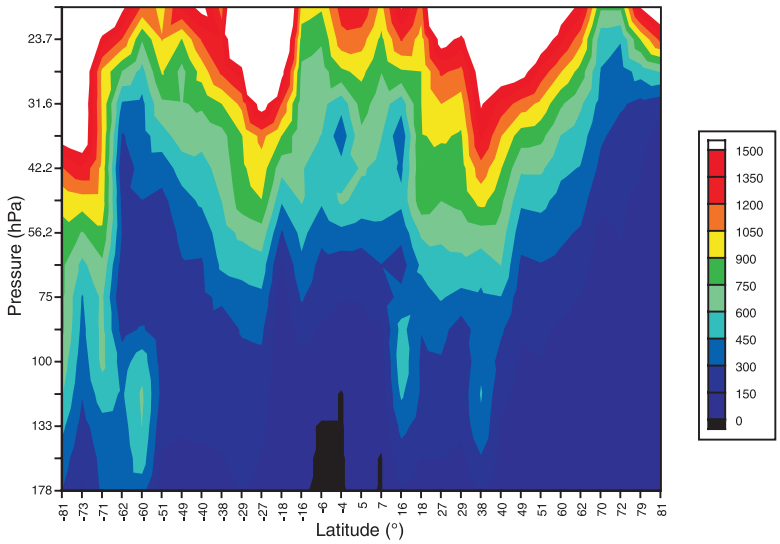

longitudes, the wind direction is predominantly zonal. This second disturbance was also observed by OSIRIS (Table 1, case 4), two days after its onset.

By 12:00 UTC on 12 October, the tongue of NO_x lies at a lower altitude (Fig. 1*d*). The steady descent continues during the course of the next 24 h (Fig. 1*e*), with the tongue of high NO_x drifting downward to a pressure of 150 mb and eastward to a longitude of 165°W along a near constant latitude of ~60°S, very close to the location of the NO_x enhancement observed by OSIRIS ~4 h later (Fig. 2). Figure 1*e* illustrates that the magnitude of the enhancement at 150 mb is clearly much larger than the natural variability of NO_x at 150 mb at high latitudes for this time of year.

Figure 3 is a time series of the zonal cross-sectional view of GEM NO_x VMR in 6 h steps. This time series also shows the eastward displacement of the tongue of high NO_x by the polar night jet (at a rate of >100 km/h beginning near 12:00 UTC on 10 October as shown in Fig. 3*d*), as well as its gradual descent and dilution in the lower stratosphere. This provides cross-sectional views of the tongue as well, which in the later stages (Figs. 3*g*–3*k*), appear as a circular area of high NO_x.

At 12:00 UTC on 11 October, the tongue of NO_x is simply advecting zonally, with concentrations of NO_x as high as 1.5 ppbv at ~90 hPa, separated from the high values of the middle stratosphere by a thin layer of denoxified air ($[NO_x] < 150$ pptv). This amounts to one order of magnitude variation in NO_x within ~2 km in the vertical direction at 65°S, according to the GEM simulations. For the next ~2 days, this tongue of NO_x is transported eastward by the predominantly zonal wind and concentrations within the tongue slowly decrease toward background values. By 00:00 UTC on 14 October 2003, the maximum concentration at 65°S in the pocket of high NO_x is <600 pptv (Fig. 3*k*), less than half of the concentration 54 hours earlier and six hours later, the high NO_x feature is absent at 65°S (Fig. 3*l*).

The onset of the disturbance from the meridional cross-sectional view is illustrated in Fig. 4. The denoxified state of the Antarctic lower stratosphere in late winter is shown in Fig. 4*a*. Figure 4*b* shows the transverse nature of the breaking Rossby wave, also mapped in Fig. 1*a* at 85 hPa. The rapid progress of the disturbance in bringing the elevated NO_x concentrations from the South Pole to near the edge of

Fig. 3. (*a*) (Top left) Zonal cross sections of GEM NO_x VMR (pptv) at 65°S at 00:00 UTC on 9 October 2003. (*b*) (Top right) same as (*a*), but for 12:00 UTC on 9 October. (*c–f*) same as (*a*) but sampled in steps of 12 h following time of (*b*).

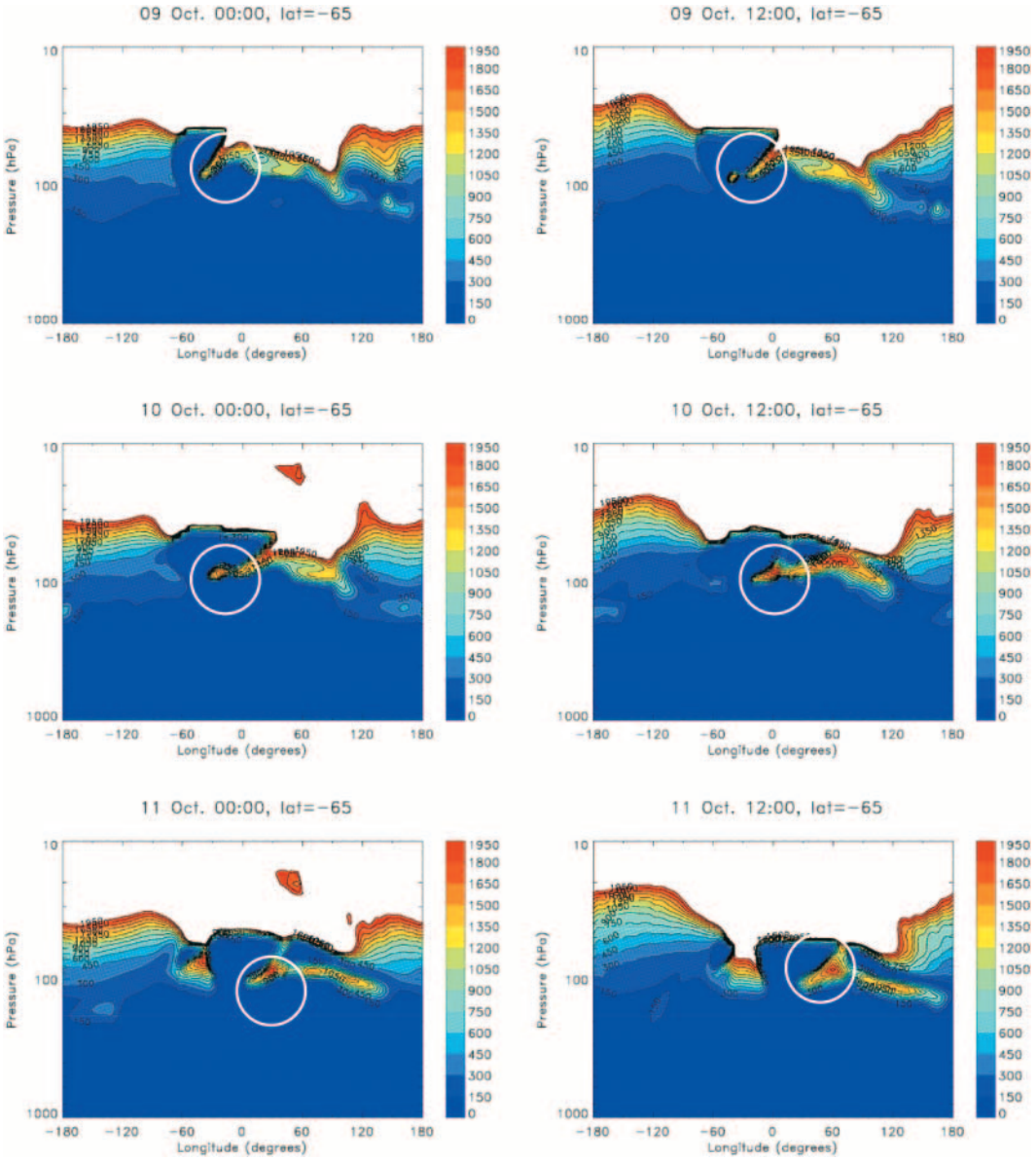

the vortex is apparent from Fig. 4*c*. A pocket of low NO_x concentrations (<150 pptv) remains above the tongue for many days and is seen by OSIRIS at 09:25 UTC on 9 October (Fig. 5).

The breaking Rossby wave is captured by OSIRIS (Fig. 5). One similarity and difference with the GEM simulations relates to the pocket of low NO_x that persists near the vortex edge, above the tongue (∼50 hPa). OSIRIS sees larger concentrations (1050±290 pptv) in the pocket of low NO_x above the tongue than simulated by GEM (<150 pptv, see Fig. 4*b*). This may be partly explained by the vertical resolution of the GEM simulations (5 hPa, which translates to ∼0.7 km at 20 km), whereas OSIRIS has

Fig. 3. (*continued*) (*g*–*k*) Continuation of time series of zonal cross sections of NO_x VMR simulated by GEM, between 00:00 UTC on 12 and 14 October 2003, at 12 h intervals. (*l*) same as (*a*), but for 06:00 UTC on 14 October.

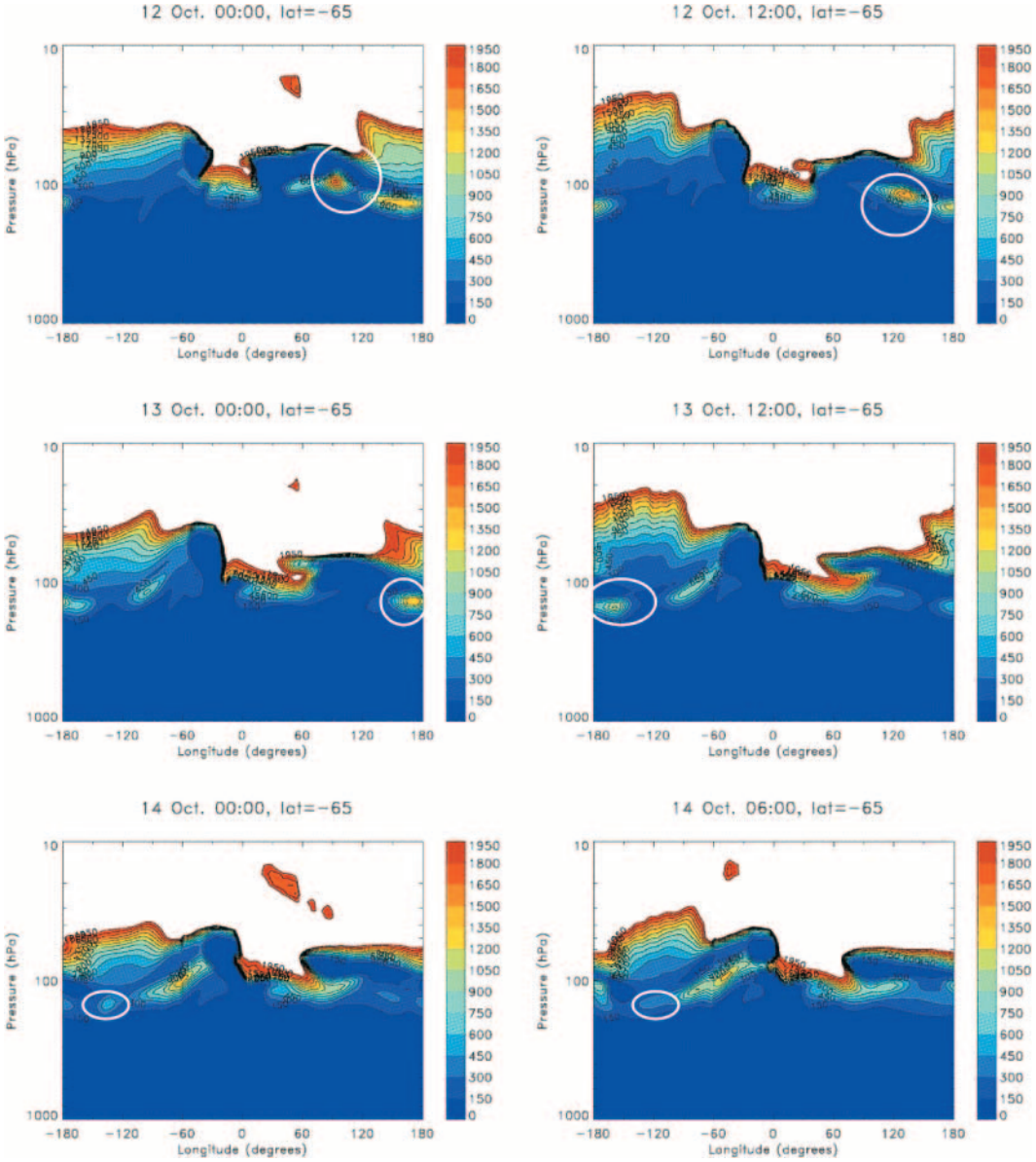

a vertical resolution of ∼2 km. Nevertheless, the OSIRIS measurements are significantly higher than the GEM simulated concentrations in this pocket of low NO_x. The underlying tongue of NO_x exhibits observed concentrations of 1790±280 pptv (Fig. 5). The GEM simulations at 06:00 (not shown) and 12:00 UTC (Fig. 3*b* and 4*b*) both show similar concentrations (1500 pptv). Quoted uncertainties on NO_x from OSIRIS are obtained by scaling NO_2 retrieval precisions (1σ) by the local NO_x/NO_2 ratio. Figure 5 also shows that the wave breaking has a slight downward component, as shown in the GEM simulations (see, for example, Figs. 3*a*–3*b*).

At 74°S, near the location of the Rossby wave breaking (see Fig. 5 caption), OSIRIS observed a

Fig. 4. (*a*) Meridional cross section of GEM NO_x VMR (pptv) at 18:00 UTC on 19 September at 30°E. (*b*) Meridional cross section of GEM NO_x VMR at the longitude of the centre of the disturbance (45°W), at 12:00 UTC on 9 October. (*c*) Same as (*b*), except for 00:00 UTC on 10 October at 15°W.

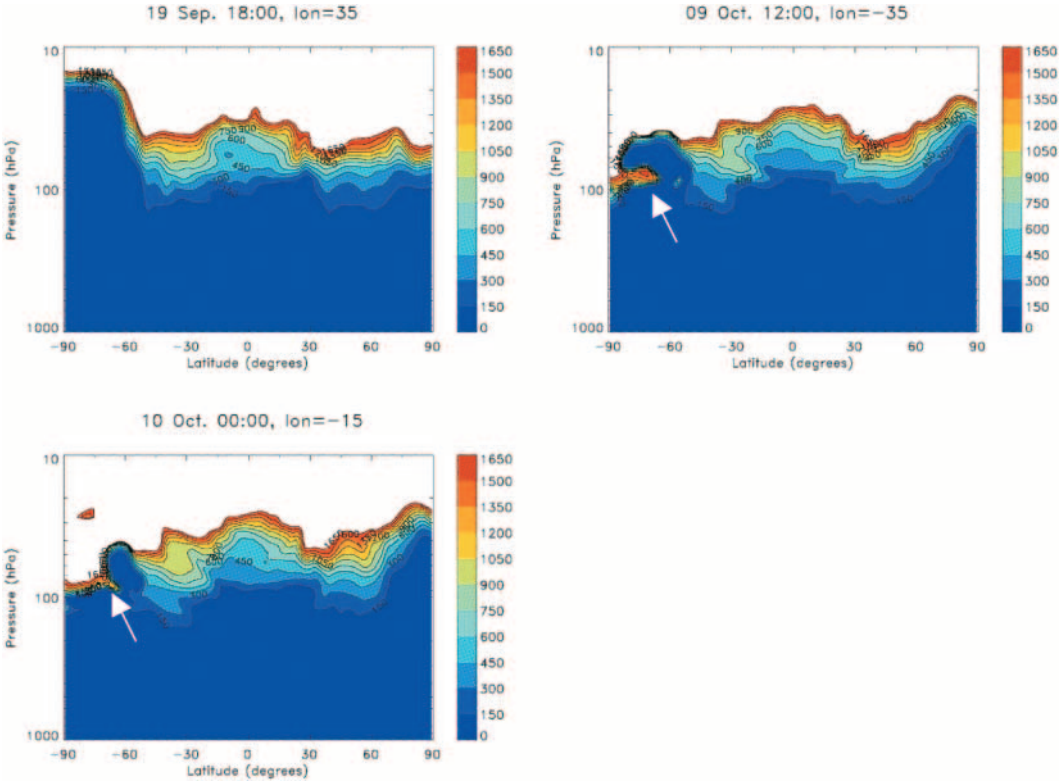

Fig. 5. Orbital cross section of NO_x VMR (pptv) from OSIRIS at southern middle and high latitudes at ∼09:25 UTC on 09 October 2003. This portion of the descending phase of the orbit is measured in 19 min. The breaking Rossby wave transports high NO_x concentrations from the pole to the vortex edge region (55–60°S) at a pressure of ∼80 hPa. Areas in black indicate missing data because of cloud interference. A limb scan at 74°S was not processed because a polar stratospheric cloud was present with the cloud top at 17.8 km (∼63 mb). Areas in white have $[NO_x] > 1.8$ ppbv. For this orbit, the latitudinal sampling is coarser (compare with Fig. 2) because OSIRIS scans are covering all mesospheric tangent heights (up to ∼100 km).

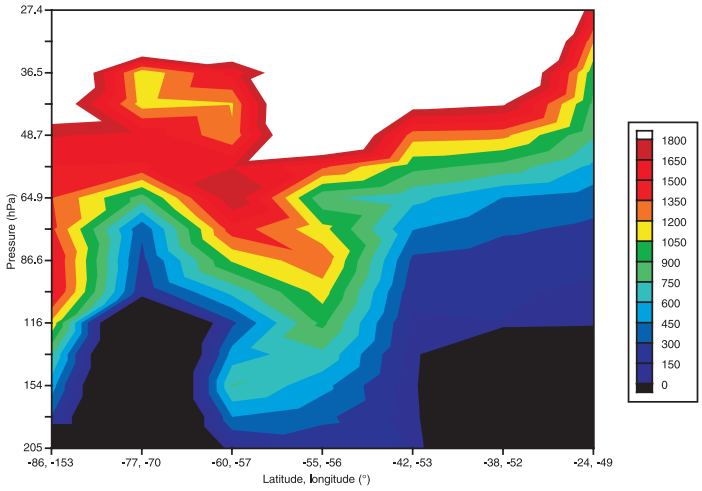

Fig. 6. (*a*) (Left) Horizontal wind velocity map (in km/h) at 00:00 UTC on 9 October 2003 at $p = 85$ hPa. (*b*) (Right) same as (*a*), but for 00:00 UTC on 12 October at $p = 100$ hPa. Colour is used to convey the magnitude of the wind velocity and the white arrows indicate the direction.

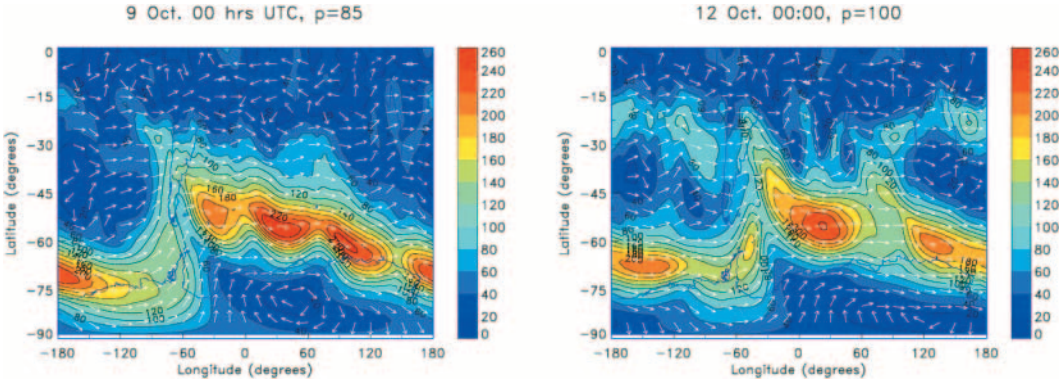

Fig. 7. Meridional cross sections of GEM NO_x (pptv) at selected longitudes at 06:00 UTC on 9 October 2003. Longitudes are 75, 65, 55, and 45°W in Figs. 7*a*–7*d*, respectively.

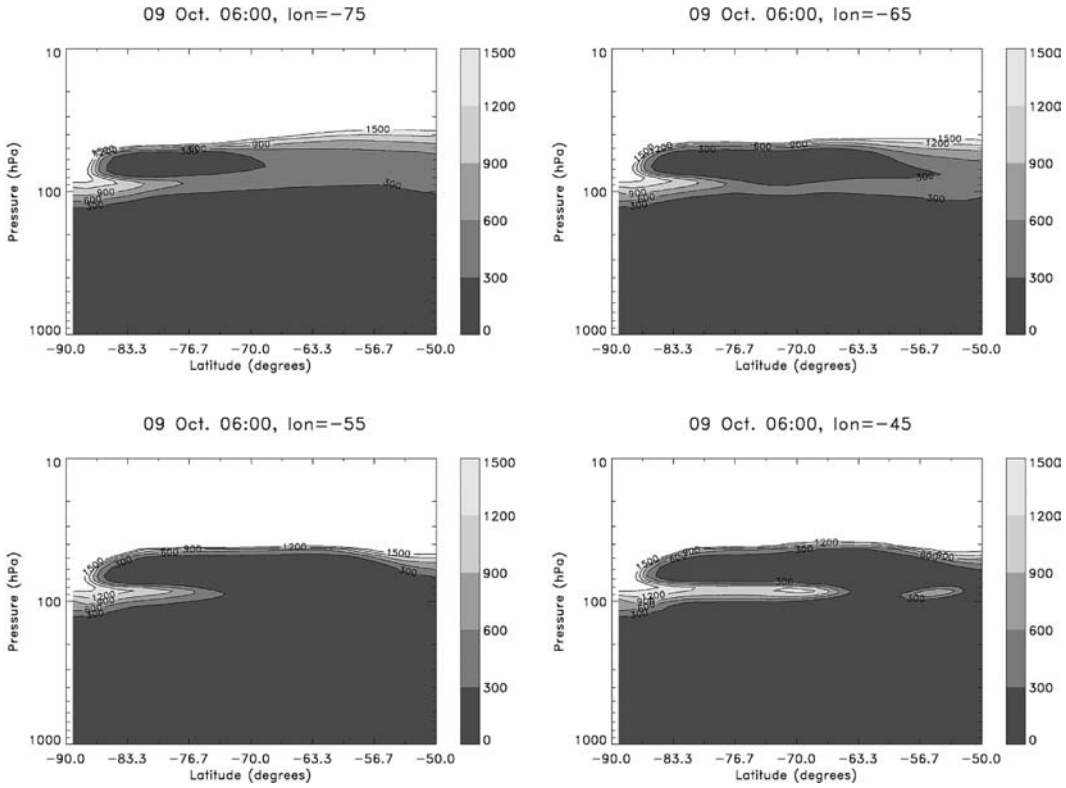

polar stratospheric cloud (PSC) at ∼18 km (with the cloud top height algorithm presented in ref. 9). The local ECMWF [11] temperature of 190.8 K at 18 km (59 mb) is below the threshold temperature for formation of type II PSCs. It is not clear without further investigation whether this extremely low temperature was partly due to a wave or simply due to the cold temperatures of the Antarctic vortex.

Figures 6*a*–6*b* map the horizontal wind velocity in the southern hemisphere at 00:00 UTC on 9 and

Fig. 8. (*a*) Close-up of tongue of NO_x (pptv) at the longitude (150°W) of its greatest latitudinal extent at 18:00 UTC on 13 October 2003. (*b*) same as (*a*), but for 135°W at 00:00 UTC on 14 October. (*c*) same as (*c*), but for 125°W at 06:00 UTC on 14 October.

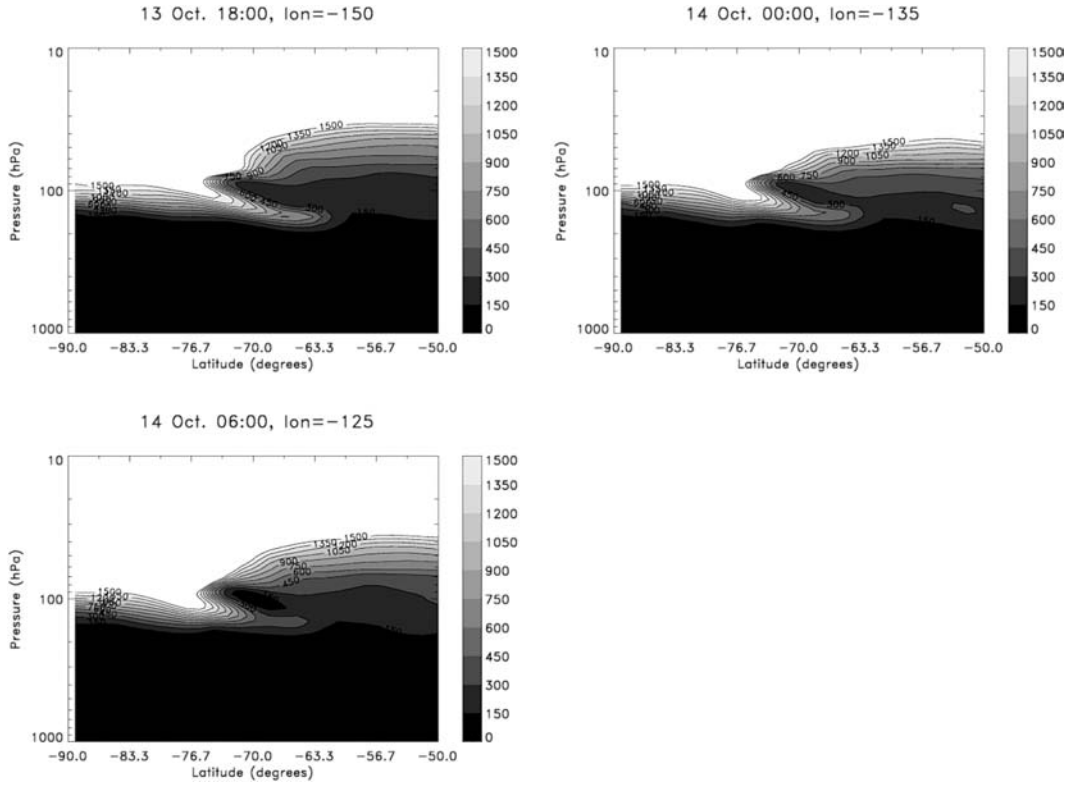

12 October 2003, respectively, in the lower stratosphere. At 65°S, the wind is predominantly zonal for the entire time period (00:00 UTC 9 October to 06:00 UTC 14 October), except in the narrow longitude range between ∼45°W and 0°. The wind field and the vortex remain relatively stationary through the entire time period studied here (00:00 on 9 October 2003 to 06:00 UTC on 14 October 2003), rotating eastward by no more than 5 to 10° of longitude per day (not shown). Kinnersley and Harwood [17] found that planetary wave breaking occurred in regions where the zonal wind velocity is less than 15 m/s. According to GEM, the zonal wind velocity at 85 hPa (not shown explicitly) was <13 m/s on 9 October 2003 (at 00:00 UTC), near the location of the breaking planetary wave (∼60°S, ∼60°W), consistent with ref. 17. At other longitudes, the polar night jet consistently has velocities greater than 15 m/s (54 km/h) throughout the entire period and major wave-breaking events are not observed.

At the onset of the wave breaking (9 Oct.), the transverse wave was present over a large range of longitudes as illustrated in Fig. 7. At 75°W (Fig. 7*a*), a pocket of low NO_x extends to 70°S above the tongue. This pocket of low NO_x matches well with the vortex edge defined by the polar night jet (Fig. 6). Heading east, the overlying pool of low NO_x air extends to lower latitudes (Figs. 7*b*–7*d*), as does the polar night jet (Fig. 6). The tongue has approximately the same latitudinal extent between 75 and 55°W (Figs. 7*a*–7*c*). At 45°W (Fig. 7*d*), the wave breaking occurs (see also Fig. 1*a*) at the point of weakness in the polar night jet.

In Fig. 8, the focus is on the GEM simulations of the decreasing concentrations and diminishing latitudinal extent of the tongue of NO_x after many days of circulating just inside the vortex edge. The receding tongue of NO_x was also seen in Fig. 3*l* as the NO_x enhancement vanished from the zonal

Fig. 9. Map of GEM $ClONO_2$ VMR (pptv) in the southern hemisphere collar and polar regions at 85 hPa on 9 October 2003 at 00:00 UTC.

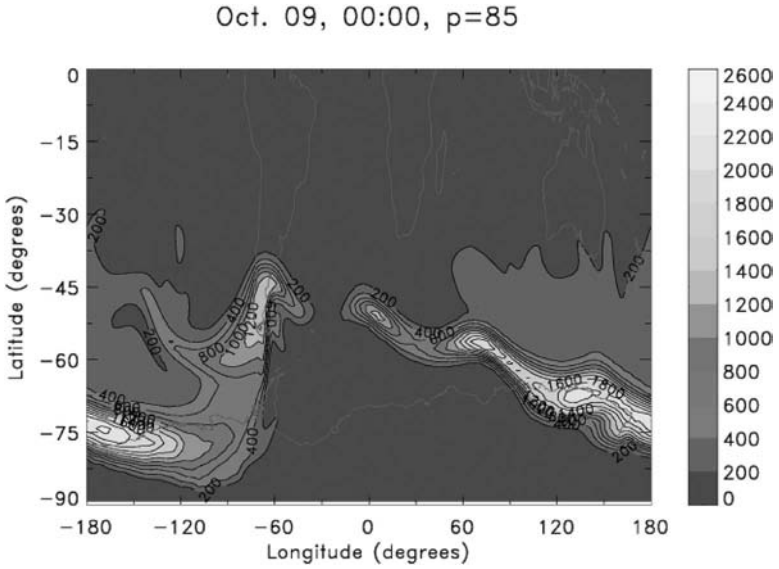

cross section at 65°S. Figure 8*a* is also presented for comparison with the NO_x meridional cross section inferred from OSIRIS observations (Fig. 2). Both the simulations and the observations show the tip of the tongue lying at a pressure of >100 mb and extending out to 60°S, with very similar NO_x concentrations at the tip of the tongue (~750 pptv). Figure 8*a* also shows that on 13 October, the NO_x concentration simulated by GEM in the minimum overlying the tongue is between 150 and 300 pptv, consistent with the 243±110 pptv of NO_x based on OSIRIS observations at 87 hPa at 62°S (see Fig. 2).

We have also considered that photodissociation of chlorine nitrate ($ClONO_2$) could produce NO_x and that the waves observed by OSIRIS and simulated by GEM could be mostly due to the photolysis of this reservoir species. We find that this is not the case. Figure 9 illustrates that $ClONO_2$ is essentially absent in the area occupied by the tongue (see Fig. 1*a*). $ClONO_2$ is abundant at the vortex edge at ≤120 hPa and is absent even in the edge region at higher pressures (not shown).

Discussion

A tongue of high NO_x in the lower stratosphere extends toward the Antarctic vortex edge during an intense wave-breaking event, and persists as a small-scale feature for several days. With its eastward advection from 40°W to 135°W, the tongue travels three quarters of the circumference of the polar vortex edge (Fig. 10) in a span of ~5 days and slightly increases concentrations of NO_x in the lower stratosphere (p >100 hPa) toward the end of this period as the tongue of high NO_x air slowly mixes with the surrounding background concentrations. Figure 10 also illustrates the deformity in the vortex near 30°W at 00:00 UTC on 13 October, which persisted for many days (slowly rotating eastward from ~40°W on 00:00 UTC on 9 October).

The second Rossby wave-breaking event, which begins near 00:00 UTC on 11 October (Fig. 3*f*), also occurs at the longitude of the vortex deformity (30°W, see Fig. 10). This inertial wave also moves along eastward in the large-scale flow for several days. Abnormally high values of NO_2 were observed by OSIRIS in the lower stratosphere at 22:49 UTC on 13 October at 101°E (see Table 1) underlying a small vertical range where much lower NO_2 concentrations were found. The inferred OSIRIS NO_x profile is consistent in terms of concentrations with the local NO_x field (Fig. 3*k*) simulated by GEM 1 h later (00:00 UTC on 14 October).

Fig. 10. (*a*) Potential vorticity map at 00:00 UTC on 13 October 2003 at southern high latitudes at $p = 85$ mb. (*b*) same as (*a*), but for 150 mb.

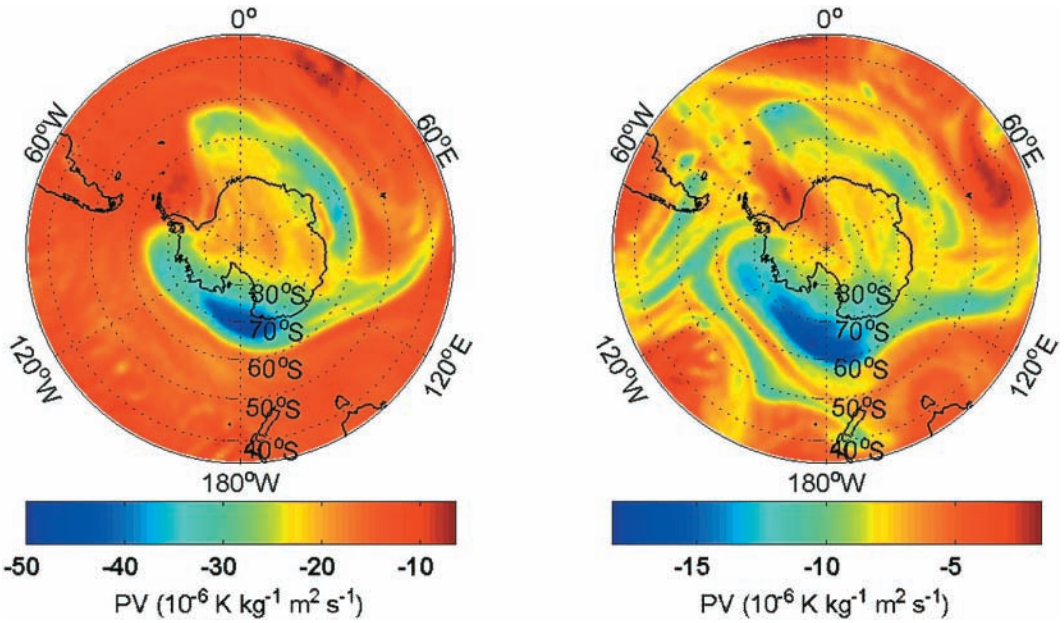

The rate of displacement of the studied tongue matches the zonal velocity of large-scale zonal flow near the vortex edge (Fig. 6). The average angular velocity of the tongue over the time period studied is ∼2°/h (i.e., well in excess of 100 km/h).

In summary, two examples are presented of Rossby wave breaking using NO_x as a dynamical tracer. The location of these events appears to coincide with a deformity in the Antarctic vortex, where the edge moves to lower latitudes within a narrow longitude range. The resulting NO_x tongues are observed by OSIRIS as they are advected zonally by the polar night jet.

Acknowledgements

We are very grateful for the guidance of Dr. Thomas Birner (University of Toronto) in interpreting the complicated dynamics of the lower part of the vortex.

References

1. C.A. McLinden, S.C. Olsen, B.J. Hannegan, O. Wild, M.J. Prather, and J. Sundet. J. Geophys. Res. **105**, 14653 (2000).
2. E.J. Llewellyn, N.D. Lloyd, D.A. Degenstein, R.L. Gattinger, S.V. Petelina, A.E. Bourassa, J.T. Wiensz, E.V. Ivanov, I.C. McDade, B.H. Solheim, J.C. McConnell, C.S. Haley, C. von Savigny, C.E. Sioris, C.A. McLinden, E. Griffioen, J. Kaminski, W.F.J. Evans, E. Puckrin, K. Strong, V. Wehrle, R.H. Hum, D.J.W. Kendall, J. Matsushita, D.P. Murtagh, S. Brohede, J. Stegman, G. Witt, G. Barnes, W.F. Payne, L. Piché, K. Smith, G. Warshaw, D.-L. Deslauniers, P. Marchand, E.H. Richardson, R.A. King, I. Wevers, W. McCreath, E. Kyrölä, L. Oikarinen, G.W. Leppelmeier, H. Auvinen, G. Mégie, A. Hauchecorne, F. Lefèvre, J. de La Nöe, P. Ricaud, U. Frisk, F. Sjoberg, F. von Schéele, and L. Nordh. Can. J. Phys. **82**, 411 (2004).
3. E.J. Bucsela, E.A. Celarier, M.O. Wenig, J.F. Gleason, J.P. Veefkind, K.F. Boersma, and E.J. Brinksma. IEEE Trans. Geosci. Remote Sens. **44**, 1245 (2006).
4. C.B. Leovy, C.-R. Sun, M.H. Hitchman, E.E. Remsberg, J.M. Russell, III, L.L. Gordley, J.C. Gille, and L.V. Lyjak. J. Atmos. Sci. **42**, 230 (1985).

5. H.L. Nordh, F. vonSchéele, U. Frisk, K. Ahola, R.S. Booth, P.J. Encrenaz, Å. Hjalmarson, D. Kendall, E. Kyrölä, S. Kwok, A. Lecacheux, G. Leppelmeier, E.J. Llewellyn, K. Mattila, G. Mégie, D. Murtagh, M. Rougeron, and G. Witt. Astron. Astrophys. **402**, L21 (2003).
6. S.M. Brohede, C.S. Haley, C.A. McLinden, C.E. Sioris, D.P. Murtagh, S.V. Petelina, E.J. Llewellyn, A. Bazureau, F. Goutail, C.E. Randall, J.D. Lumpe, G. Taha, L.W. Thomasson, and L.L. Gordley. J. Geophys. Res. **112**, D07310 (2007); doi:10.1029/2006JD007586.
7. C.S. Haley, S.M. Brohede, C.E. Sioris, E. Griffioen, D.P. Murtagh, I.C. McDade, P. Eriksson, E.J. Llewellyn, A. Bazureau, and F. Goutail. J. Geophys. Res. **109**, D16303 (2004); doi:10.1029/2004JD004588.
8. C.E. Sioris, C.S. Haley, C.A. McLinden, C. von Savigny, I.C. McDade, J.C. McConnell, W.F.J. Evans, N.D. Lloyd, E.J. Llewellyn, K.V. Chance, T.P. Kurosu, D. Murtagh, U. Frisk, K. Pfeilsticker, H. Bösch, F. Weidner, K. Strong, J. Stegman, and G. Mégie. J. Geophys. Res. **108**(D7), 4215 (2002); doi:10.1029/2002JD002672.
9. C.E. Sioris, C.A. McLinden, R.V. Martin, B. Sauvage, C.S. Haley, N.D. Lloyd, E.J. Llewellyn, P.F. Bernath, C.D. Boone, S. Brohede, and C.T. McElroy. Atmos. Chem. Phys. **7**, 4281 (2007).
10. C.S. Haley and S.M. Brohede. Can. J. Phys. **85** (2007). This issue.
11. S.M. Uppala, P.W. Kållberg, A.J. Simmons, U. Andrae, V. da Costa Bechtold, M. Fiorino, J.K. Gibson, J. Haseler, A. Hernandez, G.A. Kelly, X. Li, K. Onogi, S. Saarinen, N. Sokka, R.P. Allan, E. Andersson, K. Arpe, M.A. Balmaseda, A.C.M. Beljaars, L. van de Berg, J. Bidlot, N. Bormann, S. Caires, F. Chevallier, A. Dethof, M. Dragosavac, M. Fisher, M. Fuentes, S. Hagemann, E. Hólm, B.J. Hoskins, L. Isaksen, P.A.E.M. Janssen, R. Jenne, A.P. McNally, J.-F. Mahfouf, J.-J. Morcrette, N.A. Rayner, R.W. Saunders, P. Simon, A. Sterl, K.E. Trenberth, A. Untch, D. Vasiljevic, P. Viterbo, and J. Woollen Q. J. R. Meteorol. Soc. **131**, 2961 (2005).
12. C. Roth, D.A. Degenstein, A.E. Bourassa, and E.J. Llewellyn. Can. J. Phys. **85** (2007). This issue.
13. S. Brohede, C.A. McLinden, G. Berthet, C.S. Haley, D. Murtagh, and C.E. Sioris. Can. J. Phys. **85** (2007). This issue.
14. J. Côté, S. Gravel, A. Méthot, A. Patoine, M. Roch, and A. Staniforth. Mon. Wea. Rev. **126**, 1373 (1998).
15. F. Daerden, N. Larsen, S. Chabrillat, Q. Errera, S. Bonjean, D. Fonteyn, K. Hoppel and M. Fromm. Atmos. Chem. Phys. Discuss. **6**, 8511 (2006).
16. C. Vigouroux, M. De Mazière, Q. Errera, S. Chabrillat, E. Mahieu, P. Duchatelet, S. Wood, D. Smale, S. Mikuteit, T. Blumenstock, F. Hase and N. Jones, Atmos. Chem. Phys. **7**, 377 (2007).
17. J.S. Kinnersley and R.S. Harwood. Q. J. R. Meteorol. Soc. **119**, 1167 (1993).